ASME Open Journal of Engineering
Online journal at:
https://asmedigitalcollection.asme.org/openengineering

Julia Clarin
Mem. ASME
Department of Bioengineering,
Northeastern University,
Boston, MA 02115
e-mail: clarin.j@northeastern.edu

Dominique Dang
Department of Bioengineering,
Northeastern University,
Boston, MA 02115

Lucas Santos
Department of Bioengineering,
Northeastern University,
Boston, MA 02115

Rouzbeh Amini[1]
Mem. ASME
Department of Mechanical and Industrial Engineering;
Department of Bioengineering,
Northeastern University,
Boston, MA 02115
e-mail: r.amini@northeastern.edu

Mechanical Characterization of Porcine Tricuspid Valve Anterior Leaflets Over Time: Applications to Ex Vivo Studies

Mechanical characterization of the ex vivo tricuspid valve (TV) continues to provide key insights into native valve function and the development of valvular diseases. However, experimental methods to characterize TV biomechanical behavior ex vivo often fail to account for potential changes in the tissue's mechanical responses that may occur during experiment preparation. Therefore, we assessed the mechanical responses of the anterior tricuspid leaflet (ATL) via biaxial mechanical testing over the course of 5 h to validate the accuracy of our fresh tissue experiments. We hypothesized that ATL mechanical responses would remain consistent for the proposed time scale. We found that ATL stiffness, represented by the upper tangent modulus (UTM), did not significantly change in either the radial or circumferential directions for the 5-h test period. Similarly, no significant change was observed in radial or circumferential strains corresponding to an estimated mean systolic stress value of 85 kPa. Overall mean UTM (±standard error of the mean (SEM)) showed that ATL samples were significantly stiffer in the circumferential direction (11.3 ± 0.98 MPa) compared to the radial direction (2.29 ± 0.20 MPa) across all time points. Thus, our results indicate that the outcomes of ex vivo tricuspid valve studies requiring sample preparation up to 5 h remain reliable. [DOI: 10.1115/1.4062477]

Keywords: biomechanics, cardiovascular engineering, heart valve biomechanics

1 Introduction

The tricuspid valve (TV) contributes to overall heart function by regulating blood flow from the right atrium to the right ventricle. TV function is heavily influenced by the mechanical behavior of its leaflets and related valvular structures. For example, TV regurgitation occurs when the leaflets fail to properly coapt, leading to backflow of blood across the valve and increased strain on the heart. If left untreated, TV regurgitation can accelerate the development of more serious heart conditions such as progressive right ventricular failure [1,2]. However, high operative mortality rates and contrasting opinions on surgical approaches severely limit treatment options for over 1.6 million people in the US affected by tricuspid regurgitation [1,3–6].

Hence, researchers have turned to biomechanical approaches to characterize the complex mechanical behavior of the TV and gain insight into the pathophysiology of TV regurgitation. In an increasing number of studies, ex vivo experiments [7–12] and computational simulations [13–17] have been used to quantitatively describe and predict the mechanical properties and function of cardiac valves.

Ex vivo approaches are of particular interest in this study, as we have previously investigated porcine TV biomechanics in our ex vivo beating heart system [18,19]. Such a system enables us to isolate the mechanical behavior of the TV leaflets in whole hearts without requiring dissection of the valve apparatus [20–24]. In addition, ex vivo experiments provide preliminary insights for designing in vivo studies that better align with the principles of the three Rs (replacement, reduction, and refinement) [25,26]. Ex vivo experiments, however, often require relatively lengthy sample preparation and setup procedures. For example, preparation of whole-heart samples for our ex vivo TV experiments may take up to 5 h on average. Because the mechanical behavior of the tissue is essential to the experimental outcomes, preparation procedures must be performed efficiently to minimize degradation and maintain tissue integrity.

While tissue storage conditions have been more extensively studied [27–32], the effect of preparation and setup time on the mechanical properties of the tissue has not been determined in TV leaflets. Therefore, we characterized the mechanical properties of the anterior tricuspid leaflet (ATL) over a relevant time scale to validate the accuracy of our fresh tissue experiments using the ex vivo beating heart system. We evaluated porcine ATL mechanics by performing a series of biaxial mechanical tests over 5 h. We hypothesize that the mechanical properties do not significantly change at our time scale. While results of this study are important

[1]Corresponding author.

Manuscript received April 11, 2023; final manuscript received April 28, 2023; published online May 26, 2023. Assoc. Editor: Hameed Metghalchi.

to our ex vivo test system, they can further be applied to other mechanical tests on cardiac leaflet tissues [8,33–36].

2 Materials and Methods

2.1 Tissue Acquisition and Preparation. Healthy porcine hearts ($n = 7$, approximately 6 months old) were obtained from Animal Biotechnologies (Tyler, TX, USA) within 24–36 h of being harvested. To preserve tissue freshness, hearts were shipped in chilled phosphate-buffered saline (PBS) and used immediately upon arrival. The ATL was excised from the heart with directional integrity maintained, as described previously [28,37–39]. A square specimen (11×11 mm) was cut from the center of the leaflet for testing. ATL thickness was measured with a thickness gauge and the average of five measurements was reported. Suture lines were attached around the edges of the tissue, leaving a 7.6×7.6 mm square test region. Four submillimeter glass markers were placed at the center of the test region to quantify in-plane deformation using digital image correlation.

2.2 Equibiaxial Mechanical Test Procedure. Similar to our previous studies, samples were mounted onto a custom biaxial tensile machine such that the radial and circumferential directions are aligned with both axes [15,28,37–39]. Tissue samples were submerged in a PBS bath during testing to mimic physiological osmolarity and prevent tissue swelling [38]. To recreate the ex vivo testing environment [18,19], tissue samples and the PBS bath were kept at room temperature (21 °C).

Based on our most recent ex vivo beating heart tests ($n = 5$), the average time to run an experiment, from time of receival to data collection, was approximately 5 h. Thus, we performed biaxial mechanical testing over a period of 5 h to capture potential changes in ATL mechanical responses that may occur during our experiments. Tissue dissection and specimen preparation were initiated immediately upon receiving the fresh tissue and were completed in approximately 30 min. Specimen preparation was directly followed by initial mechanical testing (time = 0). The following five tests were spaced 1 h apart to ensure the tissue returned to an unloaded state between time points [40]. Samples remained submerged in the room temperature PBS bath in an unloaded state between tests.

Biaxial data were collected at all six time points using procedures consistent with our previous publications [28,37–39]. For this analysis, the stress-controlled equibiaxial loading protocol was used with a target stress of 120 kPa to ensure full engagement of collagen fibers [41–43]. The maximum target stress of 120 kPa corresponds with physiological loading conditions based on previous calculations for the average stress on the ATL in a healthy heart [37,38,44]. Each test consisted of ten continuous loading/unloading cycles: nine for preconditioning and the tenth used for analysis. Because the applied stress depends on sample thickness, it is important to note that the applied loads were unique for each sample [15].

2.3 Data Processing. Positional data obtained from tracking the fiducial markers were used to calculate the deformation gradient tensor, $\mathbf{F}$ [45]. The Green-Lagrangian strain tensor, $\mathbf{E}$, was calculated using $\mathbf{F}$ and the identity matrix, $\mathbf{I}$:

$$\mathbf{E} = \frac{1}{2}(\mathbf{F}^T\mathbf{F} - \mathbf{I}) \tag{1}$$

The first Piola-Kirchhoff stress tensors were calculated using the forces applied by the actuators [38] in the radial and circumferential directions, F_r and F_c, respectively:

$$P_{rr} = \frac{F_r}{A} \tag{2}$$

and

$$P_{cc} = \frac{F_c}{A} \tag{3}$$

where P_{rr} and P_{cc} designate normal stresses in the radial and circumferential directions, respectively. The cross-sectional area, A, was defined as the product of the specimen's unloaded length (7.6 mm) and thickness. Shear forces were assumed to be zero, as described previously [46].

To provide a comparative measure of stiffness, the upper tangent modulus (UTM) was obtained by fitting the post-transitional linear region of the equibiaxial response curve (60–120 kPa) using a least-squares approach as shown in Fig. 1. The circumferential upper tangent modulus (UTM_C) and radial upper tangent modulus (UTM_R) were defined as the slope of the fitted lines in the radial and circumferential directions, respectively [47]. As described previously [37], the physiological stress on the ATL during systole was estimated to be 85 kPa using Laplace's law for a healthy mean right ventricular pressure of 25 mmHg [48]. Hence, the corresponding radial and circumferential strains for an applied stress of 85 kPa were obtained for a physiological strain comparison.

2.4 Statistical Analysis. Results were tested for normality using the Shapiro-Wilk test and subjected to a one-way analysis of variance (ANOVA) to isolate the effect of time on the mechanical response of the ATL. Radial and circumferential results were compared for each time point with a paired Student's t-test. A value of $p \leq 0.05$ was considered significant for both tests. Results are presented as mean ± standard error of the mean (SEM). All data analyses and statistical tests were performed in MATLAB (Mathworks, Nantick, MA, USA).

3 Results

The mean mechanical response of the ATL (mean thickness = 360 ± 81 μm) was determined using equibiaxial test data from all specimens ($n = 7$) at each of the six consecutive time-steps. The mean response is represented by the averages of the first Piola-Kirchhoff stress and Green strain curves shown in Fig. 2. Visual examination of the overall biaxial mechanical response (Fig. 2) does not reveal any major differences in radial direction or circumferential direction with increasing time. While stress–strain curves remain relatively consistent in both directions, a higher degree of variability is observed in the radial direction.

Mean radial and circumferential UTMs are shown for all time points ($t = 0$–5 h) in Fig. 3. As previously described [37], physiological stress was approximated to be 85 kPa at a mean normal ventricular pressure of 25 mmHg [48]. Thus, the corresponding strain at

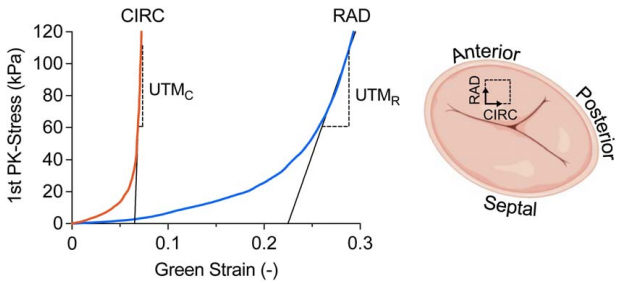

Fig. 1 Representative equibiaxial testing results with mechanical parameters for UTM_C and UTM_R obtained from fitting the circumferential (CIRC) and radial (RAD) response curves, respectively. The tricuspid valve diagram (right) indicates the region of the ATL excised for biaxial tests (square with dotted lines), where radial (RAD) and circumferential (CIRC) directions are defined with respect to ATL orientation.

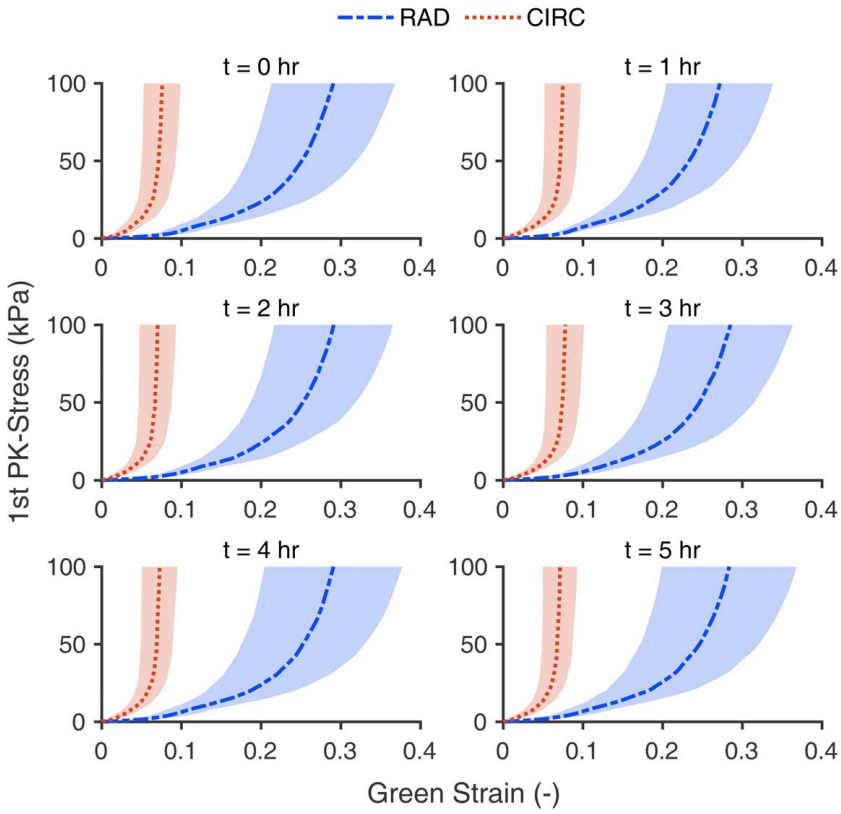

Fig. 2 First Piola-Kirchhoff stress versus Green strain curves remained consistent in the radial (RAD) and circumferential (CIRC) directions for the six consecutive time-steps of equibiaxial experiments. Each time-step shows the average stress–strain response ($n = 7$), where shaded regions indicate SEM.

stress of 85 kPa was determined to be the approximate physiological strain, as shown in Fig. 3.

A one-way ANOVA revealed that mean UTM and physiological strain did not significantly change over time in either the radial direction or circumferential direction for the 5-h test period. Overall mean circumferential stiffness was significantly higher than overall mean radial stiffness for all time points as shown in Table 1.

4 Discussion

Equibiaxial loading of the porcine ATL resulted in an anisotropic and nonlinear mechanical response that was stiffer in the circumferential direction, consistent with previous studies [37,39,43,44,47,49]. The initial un-crimping of collagen fibers translates to the initial toe region of the curves shown in Fig. 2, followed by a steeper region which signifies full collagen fiber engagement. Thus, the upper tangent moduli (UTM) provided physiologic estimates of the ATL elastic modulus.

Importantly, there was no significant difference in the mean mechanical response of the leaflets over the course of 5 h, as described by the UTM fitting in the radial and circumferential directions. The UTM was chosen as a measure of ATL stiffness to capture the mechanical response of the fiber network under physiological loading, when collagen fibers are fully engaged [44,50]. Similarly, ATL strains corresponding to a calculated mean systolic stress value (85 kPa) showed no significant change over 5 h. Collectively, these observations show that the mechanical responses of the tricuspid valve leaflets are expected to remain unchanged at short time scales, especially pertaining to ex vivo experimental setups [18,37].

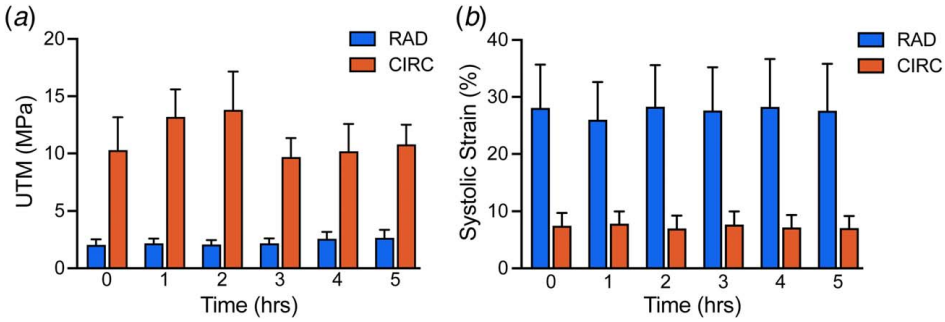

Fig. 3 Mean (*a*) UTM and (*b*) estimated systolic strain did not significantly change in the radial (RAD) and circumferential (CIRC) directions over 5 h. Error bars show SEM. Systolic strain estimates shown in (*b*) correspond to a mean systolic stress of 85 kPa, calculated previously.

Table 1 Mean UTM and physiological strain in the radial and circumferential directions for all samples presented as mean ± SEM

	Radial	Circumferential
Mean UTM (MPa)	2.29 ± 0.20	11.3 ± 0.98
Mean systolic strain (%)	27.6 ± 2.9	7.37 ± 0.85

We acknowledge that our study is not without limitations. As previously mentioned, heart samples were shipped to our lab in chilled PBS within 24–36 h of being harvested. Thus, we were unable to characterize the tissue's mechanical properties during the shipment period. However, in our previous study, we found that the mechanical properties of freshly harvested porcine ATLs remained unchanged after 2-h submersion in PBS, as evaluated with equibiaxial testing [38]. Therefore, we expect any changes in mechanical properties due to short-term storage in chilled PBS during shipment to be minimal. Furthermore, we did not characterize the ATL microstructure over time; any changes in the composition of the constituent proteins of ATL extracellular matrix were not assessed in this study. As such, our results only indicate that the tissue-level mechanical response is not affected at a time scale relevant to our ex vivo beating heart experiments.

Consistent with our proposed hypothesis, we observed that the mechanical response of the anterior tricuspid leaflet does not change significantly over a period of 5 h at room temperature. Therefore, outcomes of our ex vivo tricuspid valve studies remain reliable for tissue samples requiring up to 5 h of preparation and manipulation.

Acknowledgment

The authors acknowledge the Young Scholar's Program and the Center for STEM Education at Northeastern University for administrative support. The authors also thank Samuel D. Salinas and Fred Sebastian for providing training on mechanical test procedures and data analysis. This work was supported in part by the National Science Foundation (NSF CAREER 2049088, PI RA).

Conflict of Interest

This article does not include research in which human participants were involved. Informed consent not applicable.

Data Availability Statement

The datasets generated and supporting the findings of this article are obtainable from the corresponding author upon reasonable request.

Appendix A: Biaxial Data Analysis Exercise

As part of our commitment to broadening the impact of our research and consistent with our previous work [51,52], we have developed an educational component related to the work presented in this manuscript. In this Appendix, we have provided a learning exercise that is appropriate for a graduate-level introductory course in biomechanics or continuum mechanics. The purpose of this exercise is to practice calculating stresses and strains of a hyperelastic material using data from biaxial mechanical testing experiments presented in this work.

As described in Sec. 2.3, the positional coordinates of the four fiducial markers on the specimen's surface and the applied loads in each direction were recorded during biaxial testing. From these data, the strains and stresses applied on the tissue can be determined.

Dataset. Equibiaxial test data for one sample ($n = 1$) at the initial time point ($t = 0$ h) are provided in the Supplemental Material on the ASME Digital Collection. The first column is the time (s), the second and third columns are the applied loads (gram-force) on each side of the sample, and the remaining columns are the positions of the fiducial markers, with x_1's being the next four columns and x_2's being the last four columns. The marker positions corresponding to the lowest applied load (occurring at $t = 0.004$ s) are considered the referential marker positions. Before performing the following calculations, adjust the forces such that the first force in each column starts from 0. To do this, subtract the first force value in each column (the one that corresponds with $t = 0.004$ s) from all force values in that column. Then convert the forces to Newtons.

Problem. In the first part of this exercise, the four markers' positional coordinates are used to calculate the deformation gradient tensor, $\mathbf{F}$ [45]. Recall that the current configuration $\mathbf{x}$ and the referential configuration $\mathbf{X}$ are related to each other by the mapping function ϕ. In a two-dimensional scenario, the simplest way of such a mapping is described by

$$x_1(X_1, X_2) = a_1X_1 + b_1X_2 + c_1 \tag{A1}$$

$$x_2(X_1, X_2) = a_2X_1 + b_2X_2 + c_2 \tag{A2}$$

or in matrix form

$$\begin{Bmatrix} x_1 \\ x_2 \end{Bmatrix} = \begin{bmatrix} a_1 & b_1 & c_1 \\ a_2 & b_2 & c_2 \end{bmatrix} \begin{Bmatrix} X_1 \\ X_2 \\ 1 \end{Bmatrix} \tag{A3}$$

where the components of

$$\begin{bmatrix} a_1 & b_1 & c_1 \\ a_2 & b_2 & c_2 \end{bmatrix}$$

are constant parameters. If $\mathbf{F}$ is the deformation gradient tensor, its components can be written as

$$\begin{bmatrix} F_{11} & F_{12} \\ F_{21} & F_{22} \end{bmatrix} = \begin{bmatrix} a_1 & b_1 \\ a_2 & b_2 \end{bmatrix} \tag{A4}$$

We have no data on the third (out-of-plane) direction. However, it is safe to assume that only sample thickness changes in the out-of-plane direction, and no out-of-plane rotation occurs. Thus,

$$x_3 = \lambda_3 X_3 \tag{A5}$$

Using the assumptions given by Eqs. (A1), (A2), and (A5), and if we further assume the sample is incompressible (i.e., $\det\mathbf{F} = 1$), the deformation gradient tensor becomes

$$\mathbf{F} = \begin{bmatrix} a_1 & b_1 & 0 \\ a_2 & b_2 & 0 \\ 0 & 0 & \dfrac{1}{a_1b_2 - a_2b_1} \end{bmatrix} \tag{A6}$$

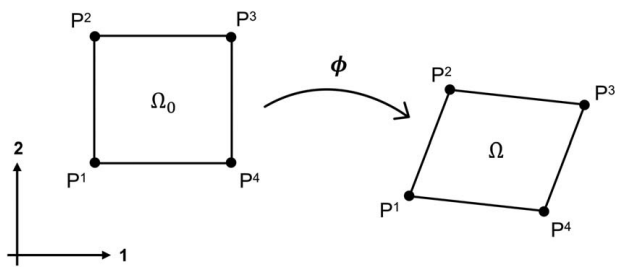

Fig. 4 Four fiducial markers identified by P^1, P^2, P^3, and P^4 are mapped from the referential configuration (Ω_0) to the deformed configuration (Ω), defined by the mapping function ϕ

Now, let us assume that we have four fiducial markers as shown in Fig. 4. If we assume that the mapping function defined by Eqs. (A1) and (A2) is identical for the entire domain Ω encompassed by the markers, we can show that

$$\begin{bmatrix} x_1^1 & x_1^2 & x_1^3 & x_1^4 \\ x_2^1 & x_2^2 & x_2^3 & x_2^4 \end{bmatrix} = \begin{bmatrix} a_1 & b_1 & c_1 \\ a_2 & b_2 & c_2 \end{bmatrix} \begin{bmatrix} X_1^1 & X_1^2 & X_1^3 & X_1^4 \\ X_2^1 & X_2^2 & X_2^3 & X_2^4 \\ 1 & 1 & 1 & 1 \end{bmatrix} \tag{A7}$$

where the superscripts refer to the number of the fiducial marker. For example, x_2^3 is the x_2 coordinate of marker P3.

Show that the approximate solution for Eq. (A7) can be written as

$$\begin{bmatrix} a_1 & b_1 & c_1 \\ a_2 & b_2 & c_2 \end{bmatrix} = [x][X^T]([X][X^T])^{-1} \tag{A8}$$

where

$$[x] = \begin{bmatrix} x_1^1 & x_1^2 & x_1^3 & x_1^4 \\ x_2^1 & x_2^2 & x_2^3 & x_2^4 \end{bmatrix} \tag{A9}$$

and

$$[X] = \begin{bmatrix} X_1^1 & X_1^2 & X_1^3 & X_1^4 \\ X_2^1 & X_2^2 & X_2^3 & X_2^4 \\ 1 & 1 & 1 & 1 \end{bmatrix} \tag{A10}$$

Using the experimental data, calculate the deformation gradient tensor $\mathbf{F}$ for all data. Then use $\mathbf{F}$ and identity tensor $\mathbf{I}$ to calculate the right Cauchy-Green deformation tensor and Green-Lagrangian strain tensor, represented by $\mathbf{C}$ and $\mathbf{E}$, respectively:

$$\mathbf{C} = \mathbf{F}^T\mathbf{F} \tag{A11}$$

$$\mathbf{E} = \frac{1}{2}(\mathbf{C} - \mathbf{I}) \tag{A12}$$

In the second part of the problem, we will determine the first Piola-Kirchhoff stress, $\mathbf{P}$. Based on our measurements, the average sample thickness at the referential configuration was approximately 0.36 mm. The load on each side was applied over a length of 7.6 mm. Thus, the undeformed area A_0 on each side of the sample can be calculated as 0.36 mm × 7.6 mm. We assume that only two components of $\mathbf{P}$ are nonzero, i.e., P_{11} and P_{22}:

$$P_{11} = \frac{f_1}{A_0} \tag{A13}$$

and

$$P_{22} = \frac{f_2}{A_0} \tag{A14}$$

where f_1 and f_2 are the forces measured in directions 1 and 2, respectively.

Calculate the stresses for all data, then plot the stresses against the strains calculated in the first part of the problem. Based on the curves presented in Fig. 2 of this paper, appropriately label the radial and circumferential directions.

References

[1] Mangieri, A., Montalto, C., Pagnesi, M., Jabbour, R. J., Rodés-Cabau, J., Moat, N., Colombo, A., and Latib, A., 2017, "Mechanism and Implications of the Tricuspid Regurgitation," Circ.: Cardiovasc. Interv., **10**(7), p. e005043.

[2] Wong, W. K., Chen, S. W., Chou, A. H., Lee, H. A., Cheng, Y. T., Tsai, F. C., and Lee, K. T., 2020, "Late Outcomes of Valve Repair Versus Replacement in Isolated and Concomitant Tricuspid Valve Surgery: A Nationwide Cohort Study," J. Am. Heart Assoc., **9**(4), p. e015637.

[3] Rogers, J. H., and Bolling, S. F., 2009, "The Tricuspid Valve: Current Perspective and Evolving Management of Tricuspid Regurgitation," Circulation, **119**(5), pp. 2718–2725.

[4] Lee, J.-W., Song, J.-M., Park, J. P., Lee, J. W., Kang, D.-H., and Song, J.-K., 2010, "Long-Term Prognosis of Isolated Significant Tricuspid Regurgitation," Circ. J. Official J. Japanese Circ. Soc., **74**(2), pp. 375–380.

[5] Chikwe, J., Itagaki, S., Anyanwu, A., and Adams, D. H., 2015, "Impact of Concomitant Tricuspid Annuloplasty on Tricuspid Regurgitation, Right Ventricular Function, and Pulmonary Artery Hypertension After Repair of Mitral Valve Prolapse," J. Am. Coll. Cardiol., **65**(5), pp. 1931–1938.

[6] Topilsky, Y., 2015, "Indications for Surgery for Tricuspid Regurgitation," Interv. Cardiol., **10**(3), pp. 58–60.

[7] Pierce, E. L., Sadri, V., Ncho, B., Kohli, K., Shah, S., and Yoganathan, A. P., 2019, "Novel In Vitro Test Systems and Insights for Transcatheter Mitral Valve Design, Part I: Paravalvular Leakage," Ann. Biomed. Eng., **47**(2), pp. 381–391.

[8] Agra, E. J., Suresh, K. S., He, Q., Onohara, D., Guyton, R. A., and Padala, M., 2020, "Left Ventricular Thinning and Distension in Pig Hearts as a Reproducible Ex Vivo Model of Functional Mitral Regurgitation," ASAIO J., **66**(9), pp. 1016–1024.

[9] de Hart, J., de Weger, A., van Tuijl, S., Stijnen, J. M. A., Rutten, M. C. M., and de Mol, B. A., 2011, "An Ex Vivo Platform to Simulate Cardiac Physiology: A New Dimension for Therapy Development and Assessment," Int. J. Artif. Organs, **34**(1), pp. 495–505.

[10] Leopaldi, A., Vismara, R., Lemma, M., Valerio, L., Cervo, M., Mangini, A., Contino, M., Redaelli, A., Antona, C., and Fiore, G., 2012, "In Vitro Hemodynamics and Valve Imaging in Passive Beating Hearts," J. Biomech., **45**(4), pp. 1133–1139.

[11] Jaworek, M., Piola, M., Lucherini, F., Gelpi, G., Castagna, M., Lentini, G., Antona, C., Fiore, G. B., and Vismara, R., 2017, "Functional Tricuspid Regurgitation Model in a Beating Heart Platform," ASAIO J., **63**(7), pp. 438–444.

[12] Vismara, R., Gelpi, G., Prabhu, S., Romitelli, P., Troxler, L. G., Mangini, A., Romagnoni, C., et al., 2016, "Transcatheter Edge-to-Edge Treatment of Functional Tricuspid Regurgitation in an Ex Vivo Pulsatile Heart Model," J. Am. Coll. Cardiol., **68**(9), pp. 1024–1033.

[13] Stevanella, M., Votta, E., Lemma, M., Antona, C., and Redaelli, A., 2010, "Finite Element Modelling of the Tricuspid Valve: A Preliminary Study," Med. Eng. Phys., **32**(12), pp. 1213–1223.

[14] Lee, C.-H., Rabbah, J.-P., Yoganathan, A. P., Gorman, R. C., Gorman, J. H., and Sacks, M. S., 2015, "On the Effects of Leaflet Microstructure and Constitutive Model on the Closing Behavior of the Mitral Valve," Biomech. Model. Mechanobiol., **14**(11), pp. 1281–1302.

[15] Khoiy, K. A., Pant, A. D., and Amini, R., 2018, "Quantification of Material Constants for a Phenomenological Constitutive Model of Porcine Tricuspid Valve Leaflets for Simulation Applications," ASME J. Biomech. Eng., **140**(9), p. 094503.

[16] Sadeghinia, M. J., Skallerud, B., Holzapfel, G. A., and Prot, V., 2022, "Biomechanics of Mitral Valve Leaflets: Second Harmonic Generation Microscopy, Biaxial Mechanical Tests and Tissue Modeling," Acta Biomater., **141**(3), pp. 244–254.

[17] Laurence, D. W., Johnson, E. L., Hsu, M., Baumwart, R., Mir, A., Burkhart, H. M., Holzapfel, G. A., Wu, Y., and Lee, C., 2020, "A Pilot in Silico Modeling-Based Study of the Pathological Effects on the Biomechanical Function of Tricuspid Valves," Int. J. Numer. Methods Biomed. Eng., **36**(7), p. e3346.

[18] Khoiy, K. A., Biswas, D., Decker, T. N., Asgarian, K. T., Loth, F., and Amini, R., 2016, "Surface Strains of Porcine Tricuspid Valve Septal Leaflets Measured in Ex Vivo Beating Hearts," ASME J. Biomech. Eng., **138**(11), p. 111006.

[19] Khoiy, K. A., Asgarian, K. T., Loth, F., and Amini, R., 2018, "Dilation of Tricuspid Valve Annulus Immediately After Rupture of Chordae Tendineae in Ex-Vivo Porcine Hearts," PLoS One., **13**(11), p. e0206744.

[20] Weston, M. W., and Yoganathan, A. P., 2001, "Biosynthetic Activity in Heart Valve Leaflets in Response to In Vitro Flow Environments," Ann. Biomed. Eng., **29**(9), pp. 752–763.

[21] Padala, M., Sacks, M. S., Liou, S. W., Balachandran, K., He, Z., and Yoganathan, A. P., 2010, "Mechanics of the Mitral Valve Strut Chordae Insertion Region," ASME J. Biomech. Eng., **132**(8), p. 081004.

[22] Brazile, B., Wang, B., Wang, G., Bertucci, R., Prabhu, R., Patnaik, S. S., and Butler, J. R., 2015, "On the Bending Properties of Porcine Mitral, Tricuspid, Aortic, and Pulmonary Valve Leaflets," J. Long-Term Eff. Med. Implants, **25**(1-2), pp. 41–53.

[23] Fatemifar, F., Feldman, M. D., Oglesby, M., and Han, H.-C., 2019, "Comparison of Biomechanical Properties and Microstructure of Trabeculae Carneae, Papillary Muscles, and Myocardium in the Human Heart," ASME J. Biomech. Eng., **141**(2), p. 021007.

[24] Zhu, Y., Imbrie-Moore, A. M., Wilkerson, R. J., Paulsen, M. J., Park, M. H., and Woo, Y. J., 2022, "Ex Vivo Biomechanical Analysis of Flexible Versus Rigid Annuloplasty Rings in Mitral Valves Using a Novel Annular Dilation System," BMC Cardiovasc. Disord., **22**(12), p. 73.

[25] Russell, W. M. S., and Burch, R. L., 1959, *The Principles of Humane Experimental Technique*, Methuen, London.

[26] Office of Laboratory Animal Welfare National Institutes of Health (US), and Applied Research Ethics National Association, 2002, *Institutional Animal Care and Use Committee Guidebook*, 2nd ed., CRC Press, Boca Raton, FL.

[27] Chow, M.-J., and Zhang, Y., 2011, "Changes in the Mechanical and Biochemical Properties of Aortic Tissue Due to Cold Storage," J. Surg. Res., **171**(12), pp. 434–442.

[28] Salinas, S. D., Clark, M. M., and Amini, R., 2020, "The Effects of 80°C Short-Term Storage on the Mechanical Response of Tricuspid Valve Leaflets," J. Biomech., **98**(1), p. 109462.

[29] Venkatasubramanian, R. T., Grassl, E. D., Barocas, V. H., Lafontaine, D., and Bischof, J. C., 2006, "Effects of Freezing and Cryopreservation on the Mechanical Properties of Arteries," Ann. Biomed. Eng., **34**(5), pp. 823–832.
[30] Stemper, B. D., Yoganandan, N., Stineman, M. R., Gennarelli, T. A., Baisden, J. L., and Pintar, F. A., 2007, "Mechanics of Fresh, Refrigerated, and Frozen Arterial Tissue," J. Surg. Res., **139**(5), pp. 236–242.
[31] Duginski, G. A., Ross, C. J., Laurence, D. W., Johns, C. H., and Lee, C.-H., 2020, "An Investigation of the Effect of Freezing Storage on the Biaxial Mechanical Properties of Excised Porcine Tricuspid Valve Anterior Leaflets," J. Mech. Behav. Biomed. Mater., **101**(1), p. 103438.
[32] Delgadillo, J. O. V., Delorme, S., El-Ayoubi, R., DiRaddo, R., and Hatzikiriakos, S. G., 2010, "Effect of Freezing on the Passive Mechanical Properties of Arterial Samples," J. Biomed. Sci. Eng., **3**(7), pp. 645–652.
[33] Kondruweit, M., Friedl, S., Heim, C., Wittenberg, T., Weyand, M., and Harig, F., 2017, "A New Ex Vivo Beating Heart Model to Investigate the Application of Heart Valve Performance Tools With a High-Speed Camera," ASAIO J., **60**(1), pp. 38–43.
[34] Easley, T. F., Bloodworth, C. H., Bhal, V., and Yoganathan, A. P., 2018, "Effects of Annular Contraction on Anterior Leaflet Strain Using an In Vitro Simulator With a Dynamically Contracting Mitral Annulus," J. Biomech., **66**(1), pp. 51–56.
[35] Imbrie-Moore, A. M., Park, M. H., Paulsen, M. J., Sellke, M., Kulkami, R., Wang, H., Zhu, Y., et al., 2020, "Biomimetic Six-Axis Robots Replicate Human Cardiac Papillary Muscle Motion: Pioneering the Next Generation of Biomechanical Heart Simulator Technology," J. R. Soc. Int., **17**(12), p. 20200614.
[36] Park, C., Fan, Y., Hager, G., Yuk, H., Singh, M., Rojas, A., and Hameed, A., 2020, "An Organosynthetic Dynamic Heart Model With Enhanced Biomimicry Guided by Cardiac Diffusion Tensor Imaging," Sci. Robot., **5**(1), p. eaay9106.
[37] Khoiy, K. A., and Amini, R., 2016, "On the Biaxial Mechanical Response of Porcine Tricuspid Valve Leaflets," ASME J. Biomech. Eng., **138**(10), p. 104504.
[38] Salinas, S. D., Clark, M. M., and Amini, R., 2019, "Mechanical Response Changes in Porcine Tricuspid Valve Anterior Leaflet Under Osmotic-induced Swelling," Bioengineering, **6**(8), p. 70.
[39] Salinas, S. D., Farra, Y. M., Khoiy, K. A., Houston, J., Lee, C.-H., Bellini, C., and Amini, R., 2022, "The Role of Elastin on the Mechanical Properties of the Anterior Leaflet in Porcine Tricuspid Valves," PLoS One., **17**(5), p. e0267131.
[40] Grashow, J. S., Sacks, M. S., Liao, J., and Yoganathan, A. P., 2006, "Planar Biaxial Creep and Stress Relaxation of the Mitral Valve Anterior Leaflet," Ann. Biomed. Eng., **34**(10), pp. 1509–1518.
[41] Caballero, A., Sulejmani, F., Martin, C., Pham, T., and Sun, W., 2017, "Evaluation of Transcatheter Heart Valve Biomaterials: Biomechanical Characterization of Bovine and Porcine Pericardium," J. Mech. Behav. Biomed. Mater., **75**(11), pp. 486–494.
[42] Sun, W., Sacks, M. S., Sellaro, T. L., Slaughter, W. S., and Scott, M. J., 2003, "Biaxial Mechanical Response of Bioprosthetic Heart Valve Biomaterials to High In-Plane Shear," J. Biomech. Eng., **125**(6), pp. 372–380.
[43] Pokutta-Paskaleva, A., Sulejmani, F., DelRocini, M., and Sun, W., 2019, "Comparative Mechanical, Morphological, and Microstructural Characterization of Porcine Mitral and Tricuspid Leaflets and Chordae Tendineae," Acta Biomater., **85**(2), pp. 241–252.
[44] Jett, S., Laurence, D., Kunkel, R., Babu, A. R., Kramer, K., Baumwart, R., Towner, R., Wu, Y., and Lee, C.-H., 2018, "Biaxial Mechanical Data of Porcine Atrioventricular Valve Leaflets," Data Brief, **21**(12), pp. 358–363.
[45] Lake, S. P., and Barocas, V. H., 2011, "Mechanical and Structural Contribution of Non-fibrillar Matrix in Uniaxial Tension: A Collagen-Agarose Co-Gel Model," Ann. Biomed. Eng., **39**(7), pp. 1891–1903.
[46] Sacks, M. S., 2000, "Biaxial Mechanical Evaluation of Planar Biological Materials," J. Elast., **61**, pp. 199–246.
[47] Pham, T., Sulejmani, F., Shin, E., Wang, D., and Sun, W., 2017, "Quantification and Comparison of the Mechanical Properties of Four Human Cardiac Valves," Acta Biomater., **54**(5), pp. 345–355.
[48] Rubin, L. J., 1997, "Primary Pulmonary Hypertension," N. Engl. J. Med., **336**(1), pp. 111–117.
[49] Laurence, D., Ross, C., Jett, S., Johns, C., Echols, A., Baumwart, R., Towner, R., et al., 2019, "An Investigation of Regional Variations in the Biaxial Mechanical Properties and Stress Relaxation Behaviors of Porcine Atrioventricular Heart Valve Leaflets," J. Biomech., **83**(1), pp. 16–27.
[50] Jan, N.-J., and Sigal, I. A., 2018, "Collagen Fiber Recruitment: A Microstructural Basis for the Nonlinear Response of the Posterior Pole of the Eye to Increases in Intraocular Pressure," Acta Biomater., **72**(5), pp. 295–305.
[51] Thomas, V. S., Lai, V., and Amini, R., 2019, "A Computational Multi-scale Approach to Investigate Mechanically-Induced Changes in Tricuspid Valve Anterior Leaflet Microstructure," Acta Biomater., **94**(8), pp. 524–535.
[52] Nwotchouang, B. S. T., Eppelheimer, M. S., Biswas, D., Pahlavian, S. H., Zhong, X., Oshinski, J. N., Barrow, D. L., Amini, R., and Loth, F., 2021, "Accuracy of Cardiac-Induced Brain Motion Measurement Using Displacement-Encoding With Stimulated Echoes (Dense) Magnetic Resonance Imaging (MRI): A Phantom Study," Magn. Reson. Med., **85**(3), pp. 1237–1247.